Scientia Iranica B (2018) 25(2), 728–740

Sharif University of Technology
Scientia Iranica
Transactions B: Mechanical Engineering
http://scientiairanica.sharif.edu

Free vibration analysis of rotating functionally graded annular disc of variable thickness using generalized differential quadrature method

M.H. Jalali[a], B. Shahriari[b], O. Zargar[c], M. Baghani[c,*], and M. Baniassadi[c]

a. *Department of Mechanical Engineering, Isfahan University of Technology, Isfahan, Iran.*
b. *Department of Mechanical and Aerospace Engineering, Malek-Ashtar University of Technology, Isfahan, Iran.*
c. *School of Mechanical Engineering, College of Engineering, University of Tehran, Tehran, Iran.*

Received 5 June 2016; received in revised form 22 October 2016; accepted 20 February 2017

KEYWORDS
Annular plate;
Functionally graded material;
Generalized differential quadrature method;
Natural frequency.

Abstract. In this paper, free vibration analysis of rotating annular disc made of Functionally Graded Material (FGM) with variable thickness is presented. Elasticity modulus, density, and thickness of the disc are assumed to vary radially according to a power low function. The natural frequencies and critical speeds of the rotating FG annular disc of variable thickness with two types of boundary conditions are obtained employing the numerical Generalized Differential Quadrature Method (GDQM). The boundary conditions considered in the analysis are both edges clamped (C-C): the inner edge clamped and outer edge free (C-F). The influence of the graded index, thickness variation, geometric parameters, and angular velocity on the dimensionless natural frequencies and critical speeds is demonstrated. It is shown that we have higher critical speed and natural frequency using a plate with a convergent thickness profile, and lower critical speed using a divergent thickness profile. It is found that the increase in the ratio of inner-outer radii could increase the critical speed of the FG annular disk. The results of the present work could improve the design of the rotating FG annular disk in order to avoid resonance condition.

1. Introduction

Functionally Graded Materials (FGM) are a new type of composite materials, which have gained considerable attention in various industries recently. Due to the special advantages of using composite materials, some mechanical structures, such wind turbine blades, are growing in size and becoming structurally more efficient [1-3]. Mechanical properties in plates made of FG materials vary continuously in one or more directions [4,5]. Since circular plates are extensively used in many engineering applications, many researchers have performed vibration analysis of these plates.

Lamb and Southwell [6] investigated vibrations of spinning uniform disk for the first time. They obtained the natural frequencies of rotating, homogenous, constant thickness circular disk using exact solution. Southwell [7] extended the Lamb's work and analyzed the effects of rotation on the vibration of uniform homogeneous circular disk, more deeply. Deshpande and Mote [8] presented a model for in-plane vibration of rotating thin disc. Their model accounted for the stiffening of the disk due to the radial expansion resulting from its rotation. Bauer and Eidel [9] obtained the lower approximate natural frequencies of a spinning circular plate. In their paper,

*. *Corresponding author. Tel.: +98 21 6111 9921; Fax: +98 21 6600 0021*
E-mail address: baghani@ut.ac.ir (M. Baghani)

doi: 10.24200/sci.2017.4325

the plate was assumed uniform and their analysis was performed for clamped, guided and simply supported boundary conditions. Lee and Ng [10] used the assumed modes method to formulate the equations of motion of rotating homogeneous annular plates. They assumed the thickness of the plate to vary linearly and exponentially and obtained the natural frequencies and critical speeds of vibration modes consisting of radial nodal lines without any nodal circle.

Singh and Saxena [11] used Rayleigh-Ritz method to obtain the first four natural frequencies, mode shapes, and nodal radii of a circular plate. They considered the thickness variation of the plate to be exponential in radial direction and the material of the plate to be homogeneous. Taher et al. [12] analyzed the vibration of circular and annular plates with variable thickness and combined boundary conditions. In their paper, a 3D elasticity theory was used to obtain the equations, and the plates were assumed to have linear and nonlinear thickness variations.

Kermani et al. [13] used Differential Quadrature Method (DQM) to solve the equations of motion of rotating FG annular plates with constant thickness. They assumed the variation of the elasticity modulus and density of the plate to be exponential in radial direction. Horgan and Chan [14] investigated the stress in rotating functionally graded isotropic linearly elastic disks. The purpose of their paper was mainly discussing the effect of inhomogeneity on the stress in the rotating solid and annular FG disks. Nie and Batra [15] investigated the stress of the isotropic, linear thermo elastic, and incompressible FG rotating disks of variable thickness. They solved the ordinary differential equation analytically and also numerically using DQ method. Mohammadsalehi et al. [16] investigated the vibrations of variable thickness rectangular viscoelastic nano plate based on nonlocal theory. They used DQ method to solve the equations of motion and evaluated the effect of small-scale effect on the vibration features. Asghari and Ghafoori [17] presented a general semi-analytical solution for investigating elastic response of rotating solid and annular rotating FG disks. They showed that although the plane-stress solution satisfies all the governing three-dimensional equations of motion and boundary conditions, it fails to give a compatible three-dimensional strain field. Peng and Li [18] investigated the influence of orthotropy and gradient on the elastic response of the rotating annular functionally graded polar orthotropic disks. Bahaloo et al. [19] investigated the vibration and stress of a rotating functionally graded circular disk with an open circumferential crack. Khorasani and Hutton [20] investigated the vibration of rotating annular disks which were elastically restrained with rigid-body translational degrees of freedom. They discussed the effect of rotating speed on the natural frequencies of the disk and also investigated the stability of the disks thoroughly. Güven and Çelik [21] investigated the vibration of rotating functionally graded solid disks. They used Rayleigh-Ritz method to solve the equations of motion and considered the plate to be isotropic with constant thickness.

In the past few years, DQM has been applied extensively to solving engineering problems. Compared to the other numerical methods, the DQ method can lead to almost accurate results using a considerably smaller number of grid points and, hence, requiring relatively little computational effort [22,23]. The GDQ method is an improvement of the DQ method, especially for solving higher order differential equations, which is more computationally efficient and accurate. Unlike the DQ method, the GDQ method considers a general situation, where the derivatives of a function are approximated using a linear weighted sum of all the functional values and also some derivatives of the functional values [23,24]. From the above discussion on the previous papers in the literature and to the best of the authors' knowledge, the vibration analysis of rotating functionally graded thin disk with variable thickness has not been investigated so far. In this paper, the generalized differential quadrature method is used for solving the vibration equations of motion of rotating FG annular plates with variable thickness. The variation of the Young's modulus, density, and thickness of the disk in radial direction are assumed to be graded by a power-low function, and the first dimensionless natural frequency and dimensionless critical speeds are obtained. The convergence of the method is shown by the convergence diagrams, and the boundary conditions of the disk are assumed to be Clamped-Clamped (C-C) and Clamped-Free (C-F). The effects of the graded index, thickness variation, angular velocity, and geometric parameters on the first dimensionless natural frequencies and critical speeds are evaluated.

2. Governing equations for vibration analysis

An annular FG plate with outer radius, a, inner radius, b, thickness, h, and outer surface thickness, h_0, which is rotating with angular velocity, $\tilde{\omega}$, is shown in Figure 1. Thickness h can be variable in the radial direction.The equation of motion for transverse vibration of a rotating disc of variable thickness with variable material properties can be written as follows [25]:

$$D\nabla^4 w + \frac{dD}{dr}\left[2\frac{\partial}{\partial r}(\nabla^2 w) + \frac{1}{r}\left(\upsilon\frac{\partial^2 w}{\partial r^2} + \frac{1}{r}\frac{\partial w}{\partial r} + \frac{1}{r^2}\frac{\partial^2 w}{\partial \theta^2}\right)\right]$$

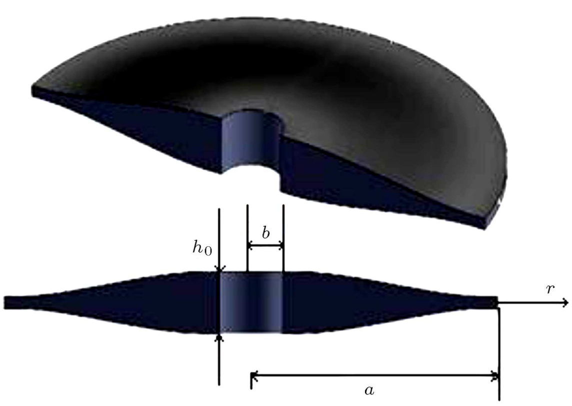

Figure 1. FG Rotating annular plate with variable thickness.

$$+\frac{d^2D}{dr^2}\left[\frac{\partial^2 w}{\partial r^2}+\upsilon\left(\frac{1}{r}\frac{\partial w}{\partial r}+\frac{1}{r^2}\frac{\partial^2 w}{\partial\theta^2}\right)\right]$$

$$-\frac{1}{r}\frac{\partial}{\partial r}\left(hr\sigma_r\frac{\partial w}{\partial r}\right)-\frac{1}{r^2}h\sigma_\theta\frac{\partial^2 w}{\partial\theta^2}+\rho h\frac{\partial^2 w}{\partial t^2}=0, \tag{1}$$

where w is the transverse deflection, D is the flexural rigidity of the disk, $D=\frac{Eh^3}{12(1-\upsilon^2)}$ $\nabla^2=\frac{\partial^2}{\partial r^2}+(\frac{1}{r})\frac{\partial}{\partial r}+\frac{1}{r^2}\frac{\partial^2}{\partial\theta^2}$ is the Laplacian operator, and σ_r and σ_θ are the radial and circumferential stresses, respectively, and are related to radial displacement by the following formula:

$$\sigma_r=\frac{E}{1-\upsilon^2}\left(\frac{du}{dr}+\frac{\upsilon u}{r}\right),$$

$$\sigma_\theta=\frac{E}{1-\upsilon^2}\left(\frac{\upsilon du}{dr}+\frac{u}{r}\right), \tag{2}$$

where E is the Young's modulus and υ is poison ratio assumed to be constant. Kirshoff strain-displacement relations lead to the expressions below:

$$\varepsilon_r=\frac{du}{dr},\qquad \varepsilon_\theta=\frac{u}{r},\qquad \gamma_{r\theta}=0, \tag{3}$$

where u is the radial displacement. The Young's modulus, density, and thickness of the disc are assumed to vary in radial direction by the following equations:

$$E=E_0\left(\frac{r}{a}\right)^n, \tag{4}$$

$$\rho=\rho_0\left(\frac{r}{a}\right)^n, \tag{5}$$

$$h=h_0\left(\frac{r}{a}\right)^{m_1}, \tag{6}$$

where n is the graded index, and m_1 is the parameter for the variation of the thickness in the radial direction. Thus:

$$D=\frac{E_0h_0^3r^{n+3m_1}}{12(1-\upsilon^2)a^{n+3m_1}}. \tag{7}$$

The following boundary conditions must be satisfied.

Clamped-Clamped (C-C):

$$r=b,\qquad w=0,\qquad \frac{\partial w}{\partial r}=0, \tag{8}$$

$$r=a,\qquad w=0,\qquad \frac{\partial w}{\partial r}=0. \tag{9}$$

Clamped-Free (C-F):

$$r=b,\qquad w=0,\qquad \frac{\partial w}{\partial r}=0, \tag{10}$$

$$r=a,$$

$$M_r=-D\left[\frac{\partial^2 w}{\partial r^2}+\upsilon\left(\frac{1}{r}\frac{\partial w}{\partial r}+\frac{1}{r^2}\frac{\partial^2 w}{\partial\theta^2}\right)\right]=0,$$

$$V_r=-D\left[\frac{\partial^3 w}{\partial r^3}+\frac{1}{r^2}\frac{\partial^2 w}{\partial r^2}-\frac{1}{r^2}\frac{\partial w}{\partial r}+\frac{2-\upsilon}{r^2}\frac{\partial^3 w}{\partial r\partial\theta^2}-\frac{3-\upsilon}{r^3}\frac{\partial^2 w}{\partial\theta^2}\right]$$

$$-\frac{dD}{dr}\left[\frac{\partial^2 w}{\partial r^2}+\upsilon\left(\frac{1}{r}\frac{\partial w}{\partial r}+\frac{1}{r^2}\frac{\partial^2 w}{\partial\theta^2}\right)\right]=0. \tag{11}$$

The transverse deflection can be written as follows:

$$w=W(r)\cos(m\theta)e^{i\omega t}, \tag{12}$$

where m is the circumferential wave number, and ω is the natural frequency. By substituting Eqs. (5)-(7), (4), and (12) into Eq. (1), the following equation of motion in terms of $W(r)$ is obtained:

$$r^{2m_1}\frac{d^4W}{dr^4}+P_1\frac{d^3W}{dr^3}+P_2\frac{d^2W}{dr^2}+P_3\frac{dW}{dr}+P_4W=0, \tag{13}$$

where:

$$P_1=2r^{2m_1-1}(n+3m_1+1),$$

$$P_2=r^{2m_1-2}(-1+(n+3m_1)(1+\upsilon+n+3m_1)-2m^2)-\frac{12a^{2m_1}}{h_0^2}\left(\frac{du}{dr}+\frac{\upsilon u}{r}\right),$$

$$P_3=r^{2m_1-3}\left((n+3m_1-1)(-1+\upsilon(n+3m_1)-2m^2)\right)-\frac{12a^{2m_1}}{h_0^2}\left((n+1+m_1)\left(\frac{1}{r}\frac{du}{dr}+\frac{\upsilon u}{r^2}\right)+\frac{d^2u}{dr^2}-\frac{\upsilon u}{r^2}+\frac{\upsilon}{r}\frac{du}{dr}\right),$$

$$P_4 = r^{2m_1-4}(m^4 - m^2(4 + (n + 3m_1)(-3 + \upsilon(n + 3m_1 - 1)))) + \frac{12m^2 a^{2m_1}}{h_0^2 r^2}\left(\frac{\upsilon du}{dr} + \frac{u}{r}\right) - \frac{12\rho_0(1-\upsilon^2)a^{2m_1}}{E_0 h_0^2}\omega^2. \tag{14}$$

In addition, the boundary equations become:

Clamped-Clamped (C-C):

$$r = b, \qquad W = 0, \qquad \frac{dW}{dr} = 0, \tag{15}$$

$$r = a, \qquad W = 0, \qquad \frac{dW}{dr} = 0. \tag{16}$$

Clamped-Free (C-F):

$$r = b, \qquad W = 0, \qquad \frac{dW}{dr} = 0, \tag{17}$$

$$r = a, \qquad \frac{d^2W}{dr^2} + \upsilon\left(\frac{1}{r}\frac{dW}{dr} - \frac{m^2}{r^2}W\right) = 0,$$

$$\frac{d^3W}{dr^3} + \frac{1 + n + 3m_1}{r}\frac{d^2W}{dr^2} + \left[\frac{-1 - m^2(2-\upsilon) + (n + 3m_1)\upsilon}{r^2}\right]\frac{dW}{dr} + \left[\frac{m^2(3-\upsilon) - (n + 3m_1)m^2\upsilon}{r^2}\right]W = 0. \tag{18}$$

Introducing the following dimensionless parameters, the motion and boundary equations can be recast in a dimensionless form as follows:

$$R = \frac{r}{a}, \qquad \bar{W} = \frac{W}{h_0}, \qquad \bar{u} = \frac{u}{h_0},$$

$$\Omega = \frac{\omega a^2}{h_0}\sqrt{\frac{12\rho_0(1-\upsilon^2)}{E_0}},$$

$$\tilde{\Omega} = \frac{\tilde{\omega} a^2}{h_0}\sqrt{\frac{12\rho_0(1-\upsilon^2)}{E_0}}. \tag{19}$$

The dimensionless equation of motion is:

$$R^{2m_1}\frac{d^4\bar{W}}{dR^4} + \bar{P}_1\frac{d^3\bar{W}}{dR^3} + \bar{P}_2\frac{d^2\bar{W}}{dR^2} + \bar{P}_3\frac{d\bar{W}}{dR} + \bar{P}_4\bar{W} = 0, \tag{20}$$

in which:

$$\bar{P}_1 = 2R^{2m_1-1}(n + 3m_1 + 1),$$

$$\bar{P}_2 = R^{2m_1-2}(-1 + (n + 3m_1)(1 + \upsilon + n + 3m_1) - 2m^2) - \frac{12a}{h_0}\left(\frac{d\bar{u}}{dR} + \frac{\upsilon\bar{u}}{R}\right),$$

$$\bar{P}_3 = R^{2m_1-3}((n + 3m_1 - 1)(-1 + \upsilon(n + 3m_1) - 2m^2)), -\frac{12a}{h_0}\left((n + 1 + m_1)\left(\frac{1}{R}\frac{d\bar{u}}{dR} + \frac{\upsilon}{R^2}\bar{u}\right) + \frac{d^2\bar{u}}{dR^2} - \frac{\upsilon\bar{u}}{R^2} + \frac{\upsilon}{R}\frac{d\bar{u}}{dR}\right),$$

$$\bar{P}_4 = R^{2m_1-4}(m^4 - m^2(4 + (n + 3m_1)(-3 + \upsilon(n + 3m_1 - 1)))) + \frac{12m^2 a}{h_0 R^2}\left(\frac{\upsilon d\bar{u}}{dR} + \frac{\bar{u}}{R}\right) - \Omega^2, \tag{21}$$

and the dimensionless boundary equations are:

Clamped-Clamped (C-C):

$$R = b/a, \qquad \bar{W} = 0, \qquad \frac{d\bar{W}}{dR} = 0, \tag{22}$$

$$R = 1, \qquad \bar{W} = 0, \qquad \frac{d\bar{W}}{dR} = 0. \tag{23}$$

Clamped-Free (C-F):

$$R = b/a, \qquad \bar{W} = 0, \qquad \frac{d\bar{W}}{dR} = 0, \tag{24}$$

$$R = 1, \qquad \frac{d^2\bar{W}}{dR^2} + \upsilon\left(\frac{1}{R}\frac{d\bar{W}}{dR} - \frac{m^2}{R^2}\bar{W}\right) = 0,$$

$$\frac{d^3\bar{W}}{dR^3} + \frac{1 + n + 3m_1}{R}\frac{d^2\bar{W}}{dR^2} + \left[\frac{-1 - m^2(2-\upsilon) + (n + 3m_1)\upsilon}{R^2}\right]\frac{d\bar{W}}{dR} + \left[\frac{m^2(3-\upsilon) - (n + 3m_1)\upsilon m^2}{R^3}\right]\bar{W} = 0. \tag{25}$$

In order to solve the equation of motion (Eq. (20)) and obtaining the dimensionless natural frequency (ω), the GDQ method is utilized.

3. Generalized Differential Quadrature Method (GDQM)

In the numerical GDQ method, the solution domain is divided into points Ri ($i = 1, 2, \cdots, N$) and derivatives of a function with the weighted summation of that function [22,23,26]. The GDQR expression for the fourth-order boundary value differential equation has been used as follows [23]:

$$\bar{W}^{(S)}(R_i) = \frac{d^s\bar{W}(R_i)}{dR^s} = \sum_{j=1}^{N+2} E_{ij}^{(S)} Uj,$$

$$i = 1, 2, \cdots, N, \tag{26}$$

where:

$$\{U_1, U_2, \cdots, U_{N+2}\} = \left\{\bar{W}_1, \bar{W}_1^{(1)}, \bar{W}_2, \cdots, \bar{W}_N, \bar{W}_N^{(1)}\right\},$$

and $\bar{W}_j$ is the function value at point j, and $\bar{W}_1^{(1)}$ and $\bar{W}_N^{(1)}$ are the first-order derivatives of the dimensionless displacement function at the first and Nth points [23]. $E_{ij}^{(S)}$ are the Sth order Weighting coefficients at points R_i. The GDQR explicit weighting coefficients have been derived in [22,23] and used directly in this paper.

In order to discretize the solution interval, two discretization schemes (I and II) are used in this paper.

I) Equally spaced points;

II) Chebyshev-Gauss-Lobatlo discretization.

$$R_i = \frac{1}{a}\left[\frac{1}{2}\left[1 - \cos\frac{(i-1)\pi}{N-1}\right](a-b) + b\right],$$

$$i = 1, 2, \cdots, N. \tag{27}$$

Appling GDQM to Eq. (20), the GDQ form of the equation of motion can be obtained as follows:

$$H_{ij}U_j = \Omega^2\bar{W}_i, \qquad i = 2, 3, \cdots, N-1, \tag{28}$$

where is a $(N)\times(N+2)$ matrix. The $(N-2)$ equations are added by four boundary equations, and $(N+2)$ algebraic equations are constructed. An assembled form is constituted by arranging them [23]:

$$\begin{bmatrix} [S_{bb}] & [S_{bd}] \\ [S_{db}] & [S_{dd}] \end{bmatrix} \begin{bmatrix} U_b \\ U_d \end{bmatrix} = \begin{bmatrix} 0 \\ \Omega^2 U_d \end{bmatrix}, \tag{29}$$

where:

$$U_b = \begin{bmatrix} \bar{W}_1 \\ \bar{W}_1^{(1)} \\ \bar{W}_N \\ \bar{W}_N^{(1)} \end{bmatrix}, \qquad U_d = \begin{bmatrix} \bar{W}_2 \\ \vdots \\ \bar{W}_{N-1} \end{bmatrix}. \tag{30}$$

By matrix substructuring and manipulation, one obtains a standard eigenvalue problem [23]:

$$[S]U_d = \Omega^2 U_d, \tag{31}$$

where:

$$[S] = [S_{dd}] - [S_{db}]\,[S_{bb}]^{-1}\,[S_{bd}],$$

with an order $(N-2)\times(N-2)$.

The dimensionless natural frequency (Ω) can be obtained by solving the eigenvalue problem (Eq. (31)).

3.1. Application of boundary conditions in GDQM

The following boundary equations are the GDQ form of Eqs. (45) and (46) for (C-C) boundary conditions.

Clamped-Clamped (C-C):

$$\bar{W}_1 = 0, \qquad U_1 = 0,$$

$$\bar{W}_1^{(1)} = 0, \qquad U_2 = 0,$$

$$\bar{W}_N = 0, \qquad U_{N+1} = 0,$$

$$\bar{W}_N^{(1)} = 0, \qquad U_{N+2} = 0. \tag{32}$$

By separating the boundary and domain coefficients in Eq. (28), we have:

$$H_{i1}U_1 + H_{i2}U_2 + H_{iN+1}U_{N+1} + H_{iN+2}U_{N+2}$$

$$+\sum_{j=3}^{N} H_{ij}U_j = \Omega^2\bar{W}_i \qquad i = 2, \cdots, N-1. \tag{33}$$

Thus, the following submatrices are obtained:

$$S_{bb} = [I]_{4*4},$$

$$S_{bd} = [0]_{4*N-2},$$

$$S_{db} = \begin{bmatrix} H_{i1} & H_{i2} & H_{iN+1} & H_{iN+2} \end{bmatrix},$$

$$i = 2, \cdots, N-1,$$

$$S_{dd} = H_{ij} \qquad i = 2, \cdots, N-1, \quad j = 3, \cdots, N. \tag{34}$$

Therefore, $S = S_{dd}$ and the eigenvalues of matrix S_{dd} are the dimensionless natural frequencies of (C-C) plate.

The following equations are the GDQ form of Eqs. (27) and (35) for (C-F) boundary conditions.

Clamped- Free (C-F):

$$\bar{W}_1 = 0, \qquad U_1 = 0,$$

$$\bar{W}_1^{(1)} = 0, \qquad U_2 = 0,$$

$$\sum_{j=1}^{N+2} E_{Nj}^{(2)} Uj + \frac{\upsilon}{R_N}\bar{W}_N^{(1)} - \frac{\upsilon m^2}{R_N^2}\bar{W}_N = 0,$$

$$\sum_{j=1}^{N+2} E_{Nj}^{(3)} U_j + \frac{1+n+3m_1}{R_N}\sum_{j=1}^{N+2} E_{Nj}^{(2)} U_j$$

$$+\left[\frac{-1-m^2(2-\upsilon)+(n+3m_1)\upsilon}{R_N^2}\right]\bar{W}_N^{(1)}$$

$$+\left[\frac{m^2(3-N)-(n+3m_1)\upsilon m^2}{R_N^3}\right]\bar{W}_N = 0. \tag{35}$$

Separating the boundary and domain coefficients in Eq. (35) and in light of Eq. (33), the following submatrices are found:

$$S_{bb}=\begin{bmatrix} 1 & 0 & 0 & 0 \\ 0 & 1 & 0 & 0 \\ E^{(2)}_{N1} & E^{(2)}_{N2} & E^{(2)}_{NN+1}-\frac{\upsilon m^2}{R_N^2} & E^{(2)}_{NN+2}+\frac{\upsilon}{R_N} \\ S_{bb1} & S_{bb2} & S_{bb3} & S_{bb4} \end{bmatrix},$$

where:

$$S_{bb1}=E^{(3)}_{N_1}+\frac{1+n+3m_1}{R_N}E^{(2)}_{N1},$$

$$S_{bb2}=E^{(3)}_{N_2}+\frac{1+n+3m_1}{R_N}E^{(2)}_{N_2},$$

$$S_{bb3}=E^{(3)}_{NN+1}+\frac{1+n+3m_1}{R_N}E^{(2)}_{NN+1}+\frac{m^2(3-\upsilon)-(n+3m_1)m^2\upsilon}{R_N^3},$$

$$S_{bb4}=E^{(3)}_{NN+2}+\frac{1+n+3m_1}{R_N}E^{(2)}_{NN+2}+\frac{-1-m^2(2-\upsilon)+(n+3m_1)\upsilon}{R_N^2}, \tag{36}$$

and:

$$S_{bd}=\begin{bmatrix} [0]_{2*4} \\ S_{bd3} \\ S_{bd4} \end{bmatrix}, \tag{37}$$

where $S_{bd3}=E^{(2)}_{Nj}$ $j=3,\cdots,N$ and $S_{bd4}=E^{(3)}_{Nj}+\frac{1+n+3m_1}{R_N}E^{(2)}_{Nj}$ $j=3,\cdots,N$. In addition, S_{db} and S_{dd} are the same as S_{db} and S_{dd} in (C-C) boundary conditions. By obtaining the dimensionless natural frequency (Ω), the natural frequency (ω) can be calculated. The obtained natural frequency is the natural frequency in the rotating (non-inertial) coordinate system, attached to the rotating plate. For each rotating plate in the rotating coordinate system, there are two corresponding natural frequencies in the stationary (inertial) coordinate system. These natural frequencies are obtained as follows [13]:

$$\omega^f=\omega+m\tilde{\omega},$$

$$\omega^b=\omega-m\tilde{\omega}, \tag{38}$$

where ω^f and ω^b are the forward and backward natural frequencies, respectively. Whenever ω^b is equal to zero, the critical speed might occur.

4. Results

Solving the eigenvalue problem of Eq. (31), the dimensionless natural frequency can be obtained for different boundary conditions. The Young's modulus and density of the plate at the outer surface are assumed to be 380 GPa and 3800 kg/m^3, respectively, and the poison ratio is assumed to be 0.3 and constant. The considered material properties are the same as those in [13] in order to validate our results compared to those in other papers in the literature.

For the discretization of the plate in the radial direction, two discretization methods are used: First equally spaced discretization (I); second, using Eq. (27) (II). Figure 2 shows the convergence diagram for the first dimensionless natural frequency using the first discretization method (equally spaced) and for (C-C) boundary conditions. As can be seen from the figure, the results could not change appreciably if the number of discrete points (N) increases between 15 and 25. Figure 3 shows the same diagram, but for Chebyshev-Gauss-Labatlo discretization (Eq. (27)). Figures 4 and 5 show the convergence diagram for (C-F) boundary conditions. It can be seen from the figures that the convergence of the method in both discretization methods is guaranteed. It should be noted that in order to obtain the out-of-plane vibration, first, the radial displacement should be calculated. In this paper, the radial displacement was first obtained using a numerical method, and the results of that were used in order to obtain the out-of-plane vibration.

In order to validate our results, Table 1 compares the first dimensionless natural frequencies obtained

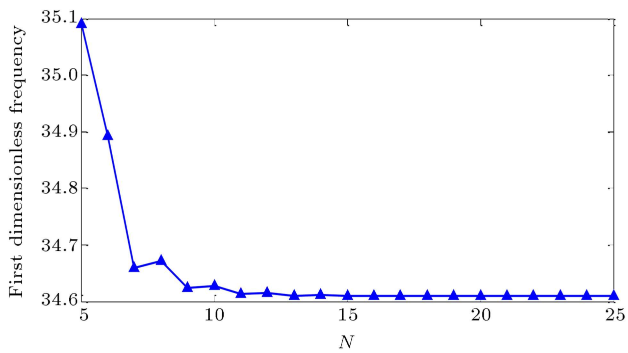

Figure 2. Convergence diagram for (C-C) boundary condition (discretization method I).

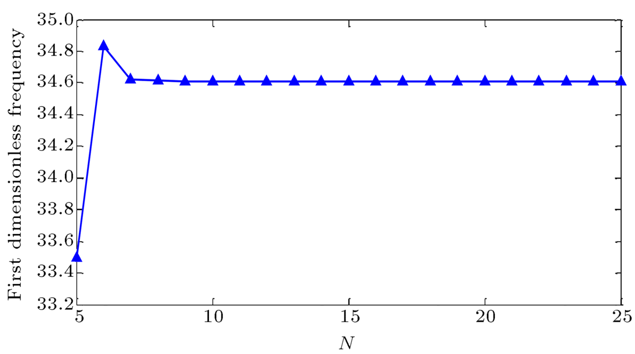

Figure 3. Convergence diagram for (C-C) boundary condition (discretization method II).

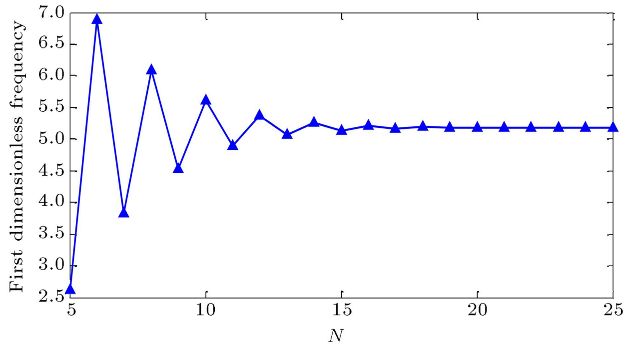

Figure 4. Convergence diagram for (C-F) boundary condition (discretization method I).

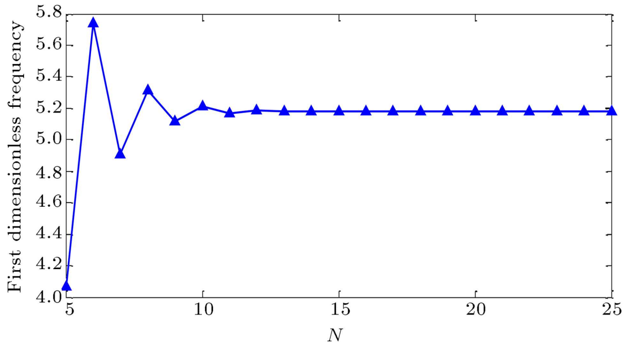

Figure 5. Convergence diagram for (C-F) boundary condition (discretization method II).

from our study with those obtained in [13]. In this table, discretization scheme is equally spaced, rotating speed is assumed to be zero, and the disc is assumed to be homogenous ($n = 0$) with the (C-C) boundary conditions. In Table 2, the same results are presented, but obtained from discretization II.

Tables 3 and 4 present the first dimensionless natural frequency for (C-F) boundary conditions using discretization I and discretization II, respectively. From Tables 1-4, we can conclude the convergence of the results, because the results are not affected sensibly by increasing (N) From 15 to 25. Also, it can validate our results, because there is good agreement between the present results and those obtained in [13]. In addition, in order to validate our results compared with those of rotating disks in the literature, the values of the first dimensionless natural frequency of the rotating homogeneous disk with (C-F) boundary conditions are presented for various inner-to-outer radii rations; thickness-to-outer radius ratio is presented in Table 5. As seen, the increase of thickness-to-outer radius ratios decreases the dimensionless natural frequencies, but the increase of inner-to-outer radii ratio increases the dimensionless natural frequencies. As obvious, the results are in good agreement with those in [13].

Figure 6 shows the variation of the first dimensionless natural frequency with the variation of the graded index for different thickness profiles for plate with clamped edges. As can be seen, the increase in value of m_1 from –1 to 1 leads to the decrease in the value of the natural frequency. Figure 7 shows the same result, but for (C-F) boundary conditions.

Figure 8 shows the variation of dimensionless forward and backward natural frequencies and that of the dimensionless rotating speed for a rotating uniform disk ($m_1 = 0$) with clamped edges. In this figure

Table 1. The lowest dimensionless natural frequency against different numbers of nodal circles for plate with (C-C) edges ($n = 0$, $m_1 = 0$, $h_0/a = 0.001$, and $b/a = 0.2$) (discretization method I).

m	0	1	2	3	4	5
Present $N = 15$	34.609	36.203	41.822	52.619	68.360	87.907
Ref. [13] $N = 15$	34.609	36.104	41.821	53.389	70.256	90.854
Present $N = 20$	34.609	36.175	41.820	52.826	68.878	88.712
Ref. [13] $N = 20$	34.609	36.103	41.820	53.388	70.256	90.855
Present $N = 25$	34.609	36.160	41.819	52.946	69.175	89.172
Ref. [13] $N = 25$	34.609	36.103	41.820	53.388	70.256	90.854

Table 2. The lowest dimensionless natural frequency against different numbers of nodal circles for plate with (C-C) edges ($n = 0$, $m_1 = 0$, $h_0/a = 0.001$, and $b/a = 0.2$) (discretization method II).

m	0	1	2	3	4	5
Present $N = 15$	34.609	36.228	41.819	52.367	67.620	87.521
Ref. [13] $N = 15$	34.609	36.104	41.821	53.389	70.256	90.854
Present $N = 20$	34.609	36.194	41.819	52.650	68.350	88.770
Ref. [13] $N = 20$	34.609	36.103	41.820	53.388	70.256	90.855
Present $N = 25$	34.609	36.174	41.819	52.811	69.765	88.384
Ref. [13] $N = 25$	34.609	36.103	41.820	53.388	70.256	90.854

Table 3. The lowest dimensionless natural frequency against different numbers of nodal circles for plate with (C-F) edges ($n = 0$, $m_1 = 0$, $h_0/a = 0.001$, and $b/a = 0.2$) (discretization method I).

m	0	1	2	3	4	5
Present $N = 15$	5.134	4.802	6.051	11.447	19.806	30.286
Ref. [13] $N = 15$	5.172	4.694	6.030	12.097	21.316	32.907
Present $N = 20$	5.185	4.939	6.502	12.099	20.551	31.115
Ref. [13] $N = 20$	5.215	4.822	6.360	12.417	21.535	33.029
Present $N = 25$	5.180	4.898	6.440	12.147	20.782	31.628
Ref. [13] $N = 25$	5.180	4.817	6.342	12.394	21.514	33.014

Table 4. The lowest dimensionless natural frequency against different numbers of nodal circles for plate with (C-F) edges ($n = 0$, $m_1 = 0$, $h_0/a = 0.001$, and $b/a = 0.2$) (discretization method II).

m	0	1	2	3	4	5
Present $N = 15$	5.180	5.006	6.441	11.588	19.558	29.607
Ref. [13] $N = 15$	5.172	4.694	6.030	12.097	21.316	32.907
Present $N = 20$	5.181	4.959	6.447	11.861	20.316	30.661
Ref. [13] $N = 20$	5.125	4.822	6.360	12.417	21.535	33.029
Present $N = 25$	5.181	4.929	6.447	12.016	20.511	31.240
Ref. [13] $N = 25$	5.213	4.817	6.342	12.394	21.514	33.014

Table 5. The lowest dimensionless natural frequency versus different inner-to-outer radii ratios and different thickness-to-outer radius ratios for the rotating functionally graded annular plate with clamped inner edge and free outer edge ($m = 0$, and $\tilde{\omega} = 1000$ rpm).

h_0/a	b/a							
	0.1		0.2		0.3		0.4	
	Present	Ref. [8]	Present	Ref. [8]	Present	Ref. [8]	Present	Ref. [8]
0.005	6.115	6.125	7.400	7.412	9.066	9.077	11.395	11.401
0.010	4.309	4.300	5.125	5.241	6.602	6.619	8.712	8.750
0.015	3.820	3.843	4.652	4.715	6.030	6.046	8.102	8.160
0.020	3.652	3.667	4.502	4.515	5.800	5.832	7.860	7.943
0.025	3.595	3.582	4.302	4.419	5.739	5.730	7.789	7.840
0.030	3.532	3.534	4.350	4.366	5.596	5.673	7.756	7.784

and also Figures 9-13, the mode shapes are denoted by (x, m) in which x indicates the number of nodal diameters and m indicates the number of nodal circles (excluding the boundary edges). It should be noted that all the results in the paper are based on zero nodal diameters. Figure 9 shows the same result for the plate with the inner edge clamped and outer edge free. As it was mentioned, whenever the backward natural frequency equals zero, the critical angular velocity occurs. Figure 10 shows the variation of the first dimensionless natural frequency for a rotating disk of variable thickness with clamped edges, and Figure 11 shows the same result for the plates with the inner edge clamped and outer edge free. Figures 12 and 13 show the variation of the dimensionless natural frequencies of a rotating FG uniform disk with that of the dimensionless rotating speed with clamped edges and clamped-free edges, respectively. The critical speed is recognized when the backward natural frequency goes to zero. At this speed, the disk has zero effective bending rigidity and cannot bear any transverse load.

From Figures 8-13, the critical speeds of the rotating plate with the corresponding material and thickness characteristics can be achieved. Table 6 presents the first dimensionless critical speed of rotating FG uniform plate with different values of graded index. It can be

Table 6. First dimensionless critical speed of rotating FG plate with clamped edges ($m_1 = 0$, and $b/a = 0.2$).

m	1	2	3	4
$n = 0$	28.474	21.017	18.231	17.754
$n = -1$	33.120	22.771	18.878	18.018
$n = 1$	25.394	19.939	17.942	17.714

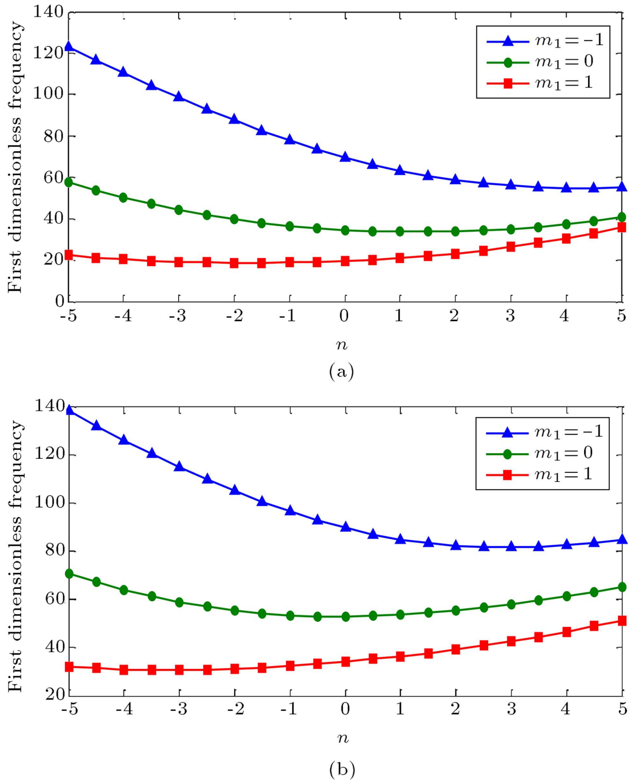

Figure 6. Fundamental natural frequency against graded index for (C-C) plate ($b/a = 0.2$, $h_o/a = 0.01$, $m = 0$, and $\tilde{\omega} = 0$).

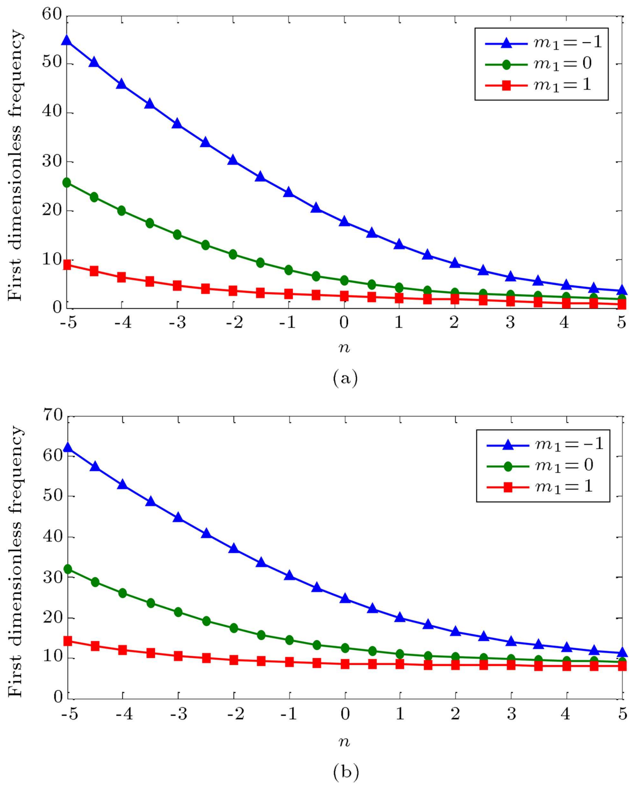

Figure 7. Fundamental natural frequency against graded index for (C-F) plate ($b/a = 0.2$, $h_o/a = 0.01$, $m = 0$, and $\tilde{\omega} = 0$).

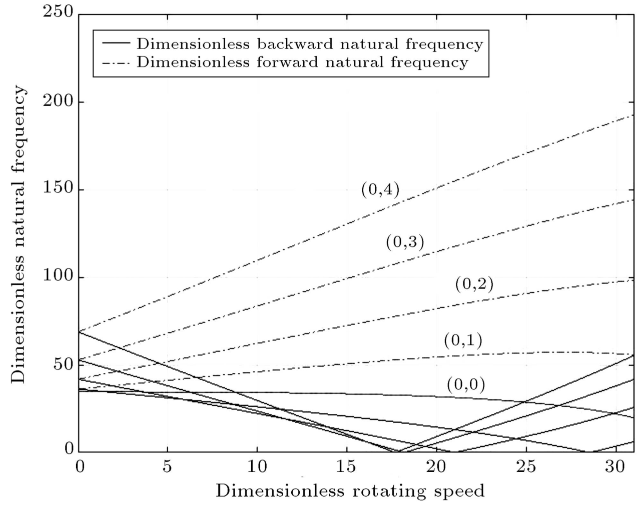

Figure 8. First dimensionless natural frequency as a function of dimensionless rotating speed for a rotating annular disk with clamped edges ($n = 0$ and $m_1 = 0$).

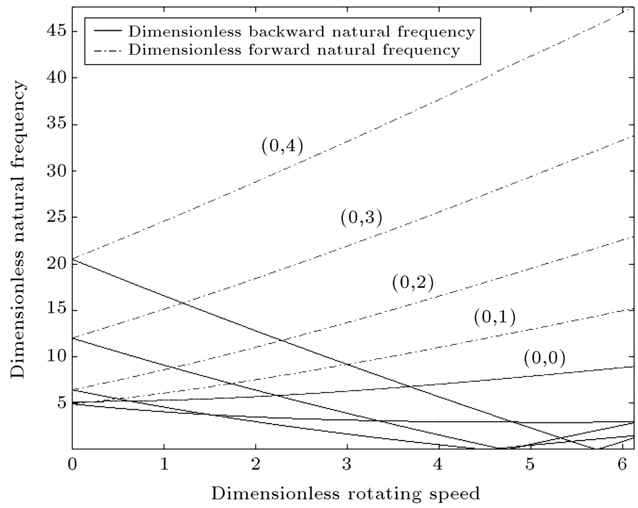

Figure 9. First dimensionless natural frequency as a function of dimensionless rotating speed for a rotating annular disk with clamped-free edges ($n = 0$ and $m_1 = 0$).

seen that the value of critical speed for $n = -1$ is larger than its value for $n = 0$ and $n = 1$.

In Table 7, the first dimensionless critical speed of the rotating FG uniform plate with (C-F) boundary conditions is presented. It should be mentioned that the critical angular velocity for the wave number one ($m = 1$) for the plate with clamped-free edges is not

Table 7. First dimensionless critical speed of rotating FG plate with clamped-free edges ($m_1 = 0$ and $b/a = 0.2$).

m	2	3	4
$n = 0$	4.510	4.756	5.772
$n = -1$	6.505	5.630	6.344
$n = 1$	3.254	4.176	5.353

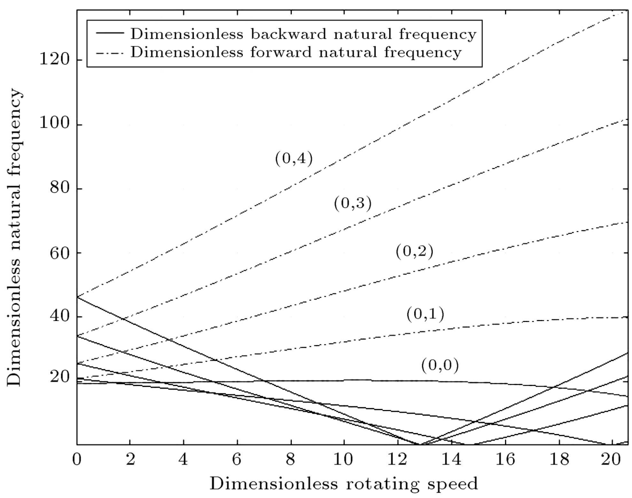

Figure 10. First dimensionless natural frequency as a function of dimensionless rotating speed for a rotating annular disk with clamped edges ($n = 0$ and $m_1 = 0$).

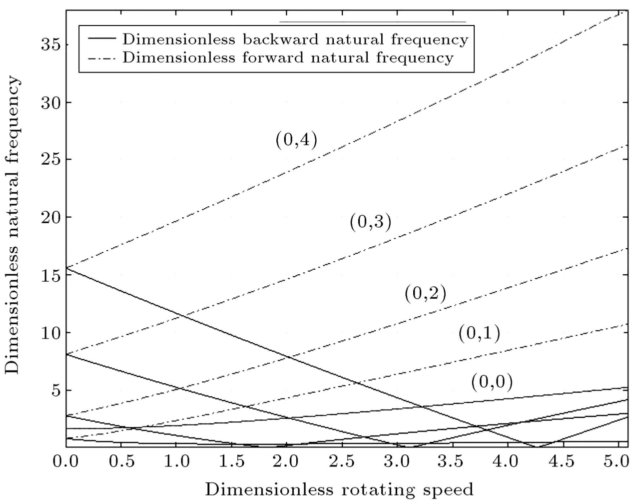

Figure 11. First dimensionless natural frequency as a function of dimensionless rotating speed for a rotating disk with clamped-free edges ($n = 0$ and $m_1 = 0$).

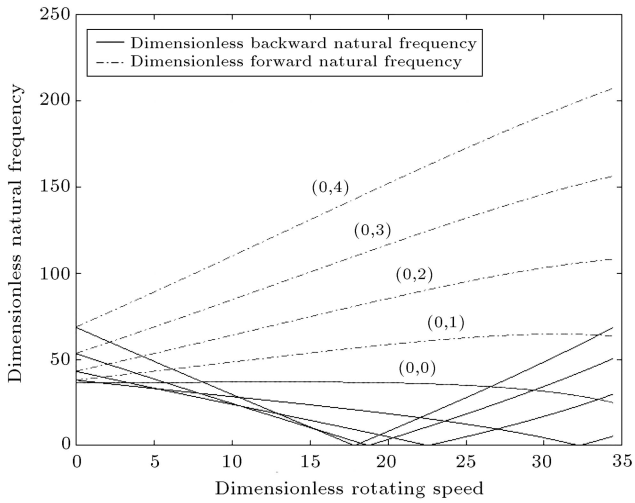

Figure 12. First dimensionless natural frequency as a function of dimensionless rotating speed for a rotating disk with clamped edges ($n = -1$ and $m_1 = 0$).

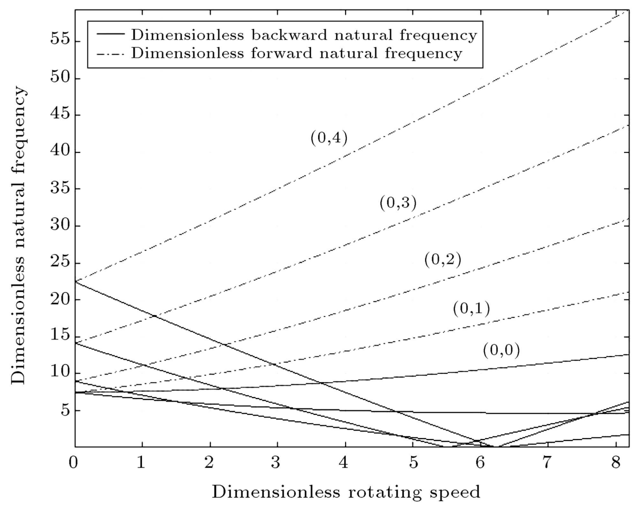

Figure 13. First dimensionless natural frequency as a function of dimensionless rotating speed for a rotating disk with clamped-free edges ($n = -1$ and $m_1 = 0$).

in the interval of the angular velocity considered in the analysis. The same results are also obtained in [13] for ($m = 1$).

In Table 8, the values of the first dimensionless critical speed for different thickness profiles and rotating homogenous plate with clamped edges are presented. Table 9 illustrates the same results, but for (C-F) boundary conditions. From Tables 8 and 9, it can be concluded that by fabricating a plate with convergent thickness profile ($m_1 = -1$), we can have a higher critical speed; by fabricating a plate with a divergent thickness profile ($m_1 = -1$), we can have a lower critical speed. This conclusion can help to improve the design of rotating FG disk in order to avoid the resonance condition.

Figure 14 shows the graph of dimensionless crit-

Table 8. First dimensionless critical speed of rotating plate with clamped edges ($n = 0$ and $b/a = 0.2$).

m	1	2	3	4
$m_1 = 0$	28.474	21.017	18.231	17.754
$m_1 = -1$	43.488	33.951	28.384	26.123
$m_1 = 1$	19.920	14.688	12.940	12.795

Table 9. First dimensionless critical speed of rotating plate with (C-F) edges ($n = 0$ and $b/a = 0.2$).

m	2	3	4
$m_1 = 0$	4.510	4.756	5.772
$m_1 = -1$	18.055	10.243	9.447
$m_1 = 1$	1.896	3.157	4.320

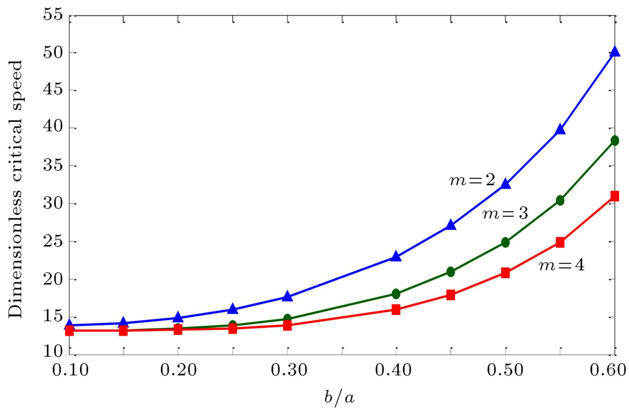

Figure 14. Dimensionless critical speed versus inner-to-outer radius ratio for C-C boundary condition.

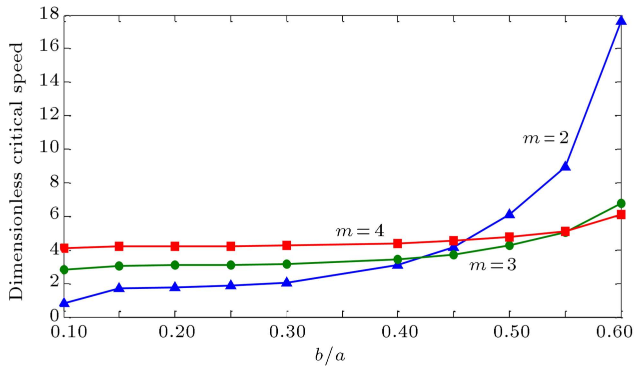

Figure 15. Dimensionless critical speed versus inner-to-outer radius ratio for C-C boundary condition.

ical speed versus the ratio of inner-to-outer radius for a FG plate with variable thickness and with clamped edges. Figure 15 shows the corresponding graph for a plate with the inner edge clamped and outer edge free. It can be seen that an increase in the inner-to-outer radii ratio could increase the critical speed. It suggests that we can have higher critical speed for the rotating annular disk if we design the annular disk with a bigger central hole with respect to the outer radius. It should be mentioned that the authors obtained their results for different values of m, n, and m_1; the same conclusion was derived.

5. Summary and conclusions

In this paper, free transverse vibration of rotating FG thin disc with variable thickness was studied. The thickness profile, elastic modulus, and density of the annular disk were considered to vary in the radial direction by a power function. The numerical generalized differential quadrature method was used to solve the equations of motion, and the convergence of the method was proved for two types of discretization methods. The effects of material and geometric parameters on the natural frequencies and critical speeds of the rotating annular FG plate with (C-C) and (C-F) boundary conditions were investigated, and the obtained results were compared with the available data from the literature; the results were validated. The obtained results can be used to improve the design of the rotating FG disk considering the avoidance of the resonance condition. It was shown that:

1. FG annular plate with a convergent thickness profile has higher critical speed than FG annular plate with uniform thickness profile, and FG annular plate with uniform thickness profile has higher critical speed than FG annular plate with a divergent thickness profile. This conclusion can be used to improve the design of the rotating FG disks in order to increase or decrease the critical speed;
2. Using a convergent thickness profile can lead to higher natural frequency than using uniform and divergent thickness profiles;
3. The increase in the ratio of inner-to-outer radius can lead to the increase in the critical speed of the rotating FG disk;
4. The increase of thickness-to-outer radius ratios decreases the dimensionless natural frequencies, but the increase of inner-to-outer radii ratio increases the dimensionless natural frequencies.

References

1. Sarrafi, A. and Mao, Z. "Statistical modeling of wavelet-transform-based features in structural health monitoring", In *Model Validation and Uncertainty Quantification*, **3**, Springer, pp. 253-262 (2016).
2. Poozesh, P., Baqersad, J., Niezrecki, C., Avitabile, P., Harvey, E., and Yarala, R. "Large-area photogrammetry based testing of wind turbine blades", *Mechanical Systems and Signal Processing*, **86**, pp. 98-115 (2017).
3. Niezrecki, C., Poozesh, P., Aizawa, K., and Heilmann, G. "Wind turbine blade health monitoring using acoustic beamforming techniques", *J. Acoust. Soc. Am.*, **135**, pp. 2392-2393 (2014).
4. Sadeghi, H., Baghani, M., and Naghdabadi, R. "Strain gradient thermoelasticity of functionally graded cylinders", *Scientia Iranica, Transactions B, Mechanical Engineering*, **21**, p. 1415 (2014).
5. Baghani, M. and Fereidoonnezhad, B. "Limit analysis of FGM circular plates subjected to arbitrary rotational symmetric loads using von-Mises yield criterion", *Acta Mechanica*, **224**, p. 1601 (2013).
6. Lamb, H. and Southwell, R. "The vibrations of a spinning disk", *Proceedings of the Royal Society of London Series A, Containing Papers of a Mathematical and Physical Character*, **99**, pp. 272-280 (1921).
7. Southwell, R. "On the free transverse vibrations of a uniform circular disc clamped at its centre; and on the effects of rotation", In *Proceedings of the Royal Society*

of London A: Mathematical, Physical and Engineering Sciences, The Royal Society, pp. 133-153 (1922).

8. Deshpande, M. and Mote, C. "In-plane vibrations of a thin rotating disk", *Journal of Vibration and Acoustics*, **125**, pp. 68-72 (2003).

9. Bauer, H.F. and Eidel, W. "Transverse vibration and stability of spinning circular plates of constant thickness and different boundary conditions", *Journal of Sound and Vibration*, **300**, pp. 877-895 (2007).

10. Lee, H. and Ng, T. "Vibration and critical speeds of a spinning annular disk of varying thickness", *Journal of Sound and Vibration*, **187**, pp. 39-50 (1995).

11. Singh, B. and Saxena, V. "Axisymmetric vibration of a circular plate with exponential thickness variation", *Journal of Sound and Vibration*, **192**, pp. 35-42 (1996).

12. Taher, H.R.D., Omidi, M., Zadpoor, A., and Nikooyan, A. "Free vibration of circular and annular plates with variable thickness and different combinations of boundary conditions", *Journal of Sound and Vibration*, **296**, pp. 1084-1092 (2006).

13. Davoodi Kermani, I., Mirdamadi, H., and Ghayour, M. "Nonlinear stability analysis of rotational dynamics and transversal vibrations of annular circular thin plates functionally graded in radial direction by differential quadrature", *Journal of Vibration and Control*, **22**, pp. 2482-2502 (2014).

14. Horgan, C. and Chan, A. "The stress response of functionally graded isotropic linearly elastic rotating disks", *Journal of Elasticity*, **55**, pp. 219-230 (1999).

15. Nie, G. and Batra, R. "Stress analysis and material tailoring in isotropic linear thermoelastic incompressible functionally graded rotating disks of variable thickness", *Composite Structures*, **92**, pp. 720-729 (2010).

16. Mohammadsalehi, M., Zargar, O., and Baghani, M. "Study of non-uniform viscoelastic nanoplates vibration based on nonlocal first-order shear deformation theory", *Meccanica*, **52** , pp. 1063-1077 (2017).

17. Asghari, M. and Ghafoori, E. "A three-dimensional elasticity solution for functionally graded rotating disks", *Composite Structures*, **92**, pp. 1092-1099 (2010).

18. Peng, X.-L. and Li, X.-F. "Elastic analysis of rotating functionally graded polar orthotropic disks", *International Journal of Mechanical Sciences*, **60**, pp. 84-91 (2012).

19. Bahaloo, H., Papadopolus, J., Ghosh, R., Mahdi, E., Vaziri, A., and Nayeb-Hashemi, H. "Transverse vibration and stability of a functionally graded rotating annular disk with a circumferential crack", *International Journal of Mechanical Sciences*, **113**, pp. 26-35 (2016).

20. Khorasany, R.M. and Hutton, S.G. "An analytical study on the effect of rigid body translational degree of freedom on the vibration characteristics of elastically constrained rotating disks", *International Journal of Mechanical Sciences*, **52**, pp. 1186-1192 (2010).

21. Güven, U. and Çelik, A. "On transverse vibrations of functionally graded isotropic linearly elastic rotating solid disks", *Mechanics Research Communications*, **28**, pp. 271-276 (2001).

22. Wu, T. and Liu, G. "A differential quadrature as a numerical method to solve differential equations", *Computational Mechanics*, **24**, pp. 197-205 (1999).

23. Wu, T. and Liu, G. "The generalized differential quadrature rule for fourth-order differential equations", *International Journal for Numerical Methods in Engineering*, **50**, pp. 1907-1929 (2001).

24. Shahriari, B., Jalali, M., and Karamooz Ravari, M. "Vibration analysis of a rotating variable thickness bladed disk for aircraft gas turbine engine using generalized differential quadrature method", *Proceedings of the Institution of Mechanical Engineers, Part G: Journal of Aerospace Engineering*, **231**, pp. 2739-2749 (2017).

25. Irie, T., Yamada, G., and Kanda, R. "Free vibration of rotating non-uniform discs: Spline interpolation technique calculations", *Journal of Sound and Vibration*, **66**, pp. 13-23 (1979).

26. Shu, C., *Differential Quadrature and Its Application in Engineering*, Springer Science & Business Media (2012).

Biographies

Mohammad Hadi Jalali received BSc and MSc degrees in Mechanical Engineering from Isfahan University of Technology in 2011 and 2013, respectively. After the graduation, he performed some industrial and academic projects in the fields of rotor dynamics and structural dynamics. His research interests are rotor dynamics, experimental modal analysis, and vibrations in rotating machinery.

Behrooz Shahriari received BSc degree in Mechanical Engineering and MSc and PhD degrees in Aerospace Engineering from Malek-Ashtar University of Technology in 2002, 2012, and 2016, respectively. He has 13 years of experience in research and doing industrial and academic projects in the fields of aerospace structural design and analysis, gas turbines, and other aerospace propulsion systems. His research interests are turbo machinery structural design/test, optimization and aerospace engines design.

Omid Zargar received BSc and MSc degrees in Mechanical Engineering from Isfahan University of Technology and Tehran University in 2012 and 2015, respectively. After the graduation, he performed some academic projects in the fields of micro and nano vibration materials (MEMS and NEMS), biomechanics and harvesting energy. His research interests are vehicle concept modeling, MEMS, experimental modal analysis, bio mechanics, and harvesting energy from piezoelectric materials.

Mostafa Baghani received his BS degree in Mechanical Engineering from University of Tehran, Iran in 2006, his MS and PhD degrees in Mechanical Engineering from the Department of Mechanical Engineering at Sharif University of Technology, Tehran, Iran in 2008 and 2012, respectively. He is now an Assistant Professor in School of Mechanical Engineering, University of Tehran. His research interests include solid mechanics, nonlinear finite-element method, and shape memory materials constitutive modeling.

Majid Baniassadi is working as an Assistant Professor in the Faculty of Mechanical Engineering at University of Tehran. He received his BSc degree from Isfahan University of Technology in 2004, his MSc from University of Tehran in 2006 and PhD from University of Strasbourg in 2011. His research interests are mainly in the area of micromechanics, nano-mechanics, and materials design.